Robust Environmental Sensing Using UAVs

AHMED BOUBRIMA and EDWARD W. KNIGHTLY, Rice University, Houston, Texas

In this article, we first investigate the quality of aerial air pollution measurements and characterize the main error sources of drone-mounted gas sensors. To that end, we build ASTRO+, an aerial-ground pollution monitoring platform, and use it to collect a comprehensive dataset of both aerial and reference air pollution measurements. We show that the dynamic airflow caused by drones affects temperature and humidity levels of the ambient air, which then affect the measurement quality of gas sensors. Then, in the second part of this article, we leverage the effects of weather conditions on pollution measurements' quality in order to design an unmanned aerial vehicle mission planning algorithm that adapts the trajectory of the drones while taking into account the quality of aerial measurements. We evaluate our mission planning approach based on a Volatile Organic Compound pollution dataset and show a high-performance improvement that is maintained even when pollution dynamics are high.

CCS Concepts: • **Computer systems organization** → **Embedded systems**; *Redundancy*; Robotics; • **Networks** → Network reliability;

Additional Key Words and Phrases: Unmanned aerial vehicles (UAVs), robust mission planning, air pollution mapping, multi-factor non-homogeneous sensing errors, experimental evaluation

ACM Reference format:
Ahmed Boubrima and Edward W. Knightly. 2021. Robust Environmental Sensing Using UAVs. *ACM Trans. Internet Things* 2, 4, Article 25 (July 2021), 20 pages.
https://doi.org/10.1145/3464943

1 INTRODUCTION

Unmanned aerial vehicles (**UAVs**), commonly known as drones, are used in many environmental applications and especially air pollution monitoring, which requires high spatial resolution sensing [4, 22]. Indeed, whether the objective is to perform a full mapping of pollution concentrations or to characterize a specific pollution plume in case of a gas leak, drones offer better spatial resolution compared to static and car-mounted sensing solutions [2]. However, due to their power constraints, drones are limited in terms of sensing resources and require efficient mission planning in order to perform measurements at the most informative sensing locations within their restricted flight time [7]. The performance of UAV mission planning algorithms highly depends on the quality of aerial sensing since low-quality measurements may lead to poor predictions of the most informative sensing locations [12].

This research was supported by Cisco, Intel, and by NSF Grant no. CNS-1801865.
Authors' address: A. Boubrima and E. W. Knightly, Electrical and Computer Engineering Department, Rice University, 6100 Main St, Houston, TX 77005, USA; emails: {ahmed.boubrima, knightly}@rice.edu.

2577-6207/2021/07-ART25 $15.00
https://doi.org/10.1145/3464943

Evaluation of pollution aerial measurements' quality. In this article, we first investigate the quality of aerial measurements of air pollution and characterize the main error sources of drone-mounted gas sensors. Although the quality of aerial pollution measurements has been studied previously [8, 24], such work provides only a qualitative evaluation and does not quantify the amount of error that is due to the main error sources, which are identified to be mainly caused by the airflow generated from the drones' propellers. In contrast, we conduct a comprehensive measurement campaign of both aerial and ground data in order to quantify the multi-factor non-homogeneous pollution sensing errors. We show that the dynamic airflow caused by drones affects first temperature and humidity levels of the ambient air, which then affect the measurement quality of gas sensors.

Without loss of generality, we focus on measuring **Volatile Organic Compound** (**VOC**) pollutants, which provide a strong signature of both industrial and traffic emissions. We build *ASTRO+*, which is an aerial-ground air pollution monitoring platform where ground sensors provide reference measurements and drones are equipped with temperature, humidity, and wind velocity sensors in addition to lightweight pollution sensors. We collect a comprehensive dataset of both aerial and ground measurements and use it to characterize the impact of weather conditions on the quality of drone-mounted pollution sensors. We show that VOC aerial measurement quality can be inferred with more than 85% accuracy based on humidity and temperature levels of the ambient air.

Robust UAV mission planning. In the second part of this article, we leverage these discovered effects of weather conditions on pollution measurements' quality in order to design a UAV mission planning algorithm that adapts the trajectory of the drones while taking into account the quality of aerial measurements that is inferred from weather conditions. Compared to most existing work [3, 13, 26–28], we consider the dynamic nature of aerial sensing errors and do not rely on static error values that are provided by manufacturers.

After a training phase prior to the flight mission in order to characterize the impact of temperature, humidity, and wind velocity on aerial measurements of pollution concentrations, our mission planning approach operates in two phases: UAVs are first sent to uniformly distributed locations in order to learn the spatial correlations of air pollution concentrations.Then in the second phase, these spatial correlations are used together with the inferred aerial measurements' quality in order to optimize the subsequent measurement locations of the drones. We evaluate our optimization approach based on our dataset of VOC measurements and show that our optimization approach is robust in the sense that low-quality measurements have a minimum impact on the selection of drones' future measurement locations.

Related Work

Characterization of the quality of pollution aerial measurements. Due to the non-instantaneous response time of pollution sensors [14], rotatory wing UAVs are preferred over fixed wing drones when performing air pollution data collection. However, when propellers are spinning, air pollution measurements are affected and their errors need to be properly characterized. Existing work focuses mainly on the qualitative evaluation of these errors. For instance, some prior work performs multiple experimental flights in an urban area and then correlates drone measurements with the proximity to traffic sources [8]. This work showed the high noise level in pollution measurements and the need of a proper characterization of measurement errors. Other prior work proposes to characterize the airflow generated by the propellers of the drones and use the wind velocity level as a qualitative indicator of pollution measurements' errors [16, 18, 24]. In contrast, we infer the measurements' errors by co-locating drones and ground sensors and then extracting the correlations between pollution data and wind in addition to temperature and humidity.

UAV mission planning for environmental mapping. Mobile sensors' mission planning for environmental monitoring in general and air pollution mapping in particular has been extensively studied in the literature [3, 13, 26–28]. Most existing work relies on the spatial correlation of air pollution concentrations: that is, closer locations have higher probability of being at the same concentration level [5, 9, 10, 19]. Based on that, the uncertainty of pollution estimation at unmeasured locations is formulated as a function of the spatial correlations of the measurements. The optimized sensing mission plan (i.e., the optimal set of sensing way-points) is then obtained by minimizing the uncertainty of pollution estimations at unmeasured locations. In contrast, and as opposed to our previous work [5] that is focused on static sensors rather than drones, we propose in this article to couple the pollution spatial correlations with a fine characterization of aerial measurements' quality in the optimization process of UAV mission planning.

Article Structure

This article extends our preliminary work presented in [6], and is organized as follows. In the next section, we present our aerial-ground air pollution monitoring system *ASTRO+*. Then in Section 3, we present our quantitative evaluation of aerial pollution measurements quality using a dataset collected with *ASTRO+*. After that, we present and evaluate our robust mission planning approach in Sections 4 and 5, respectively. Finally, we conclude the article in Section 6.

2 ASTRO+: AERIAL-GROUND AIR POLLUTION MONITORING PLATFORM

In this section, we present *ASTRO+*, an environmental sensing platform that extends our *ASTRO* drone networks system previously presented in [17]. Compared to [17], we deploy and evaluate the effectiveness of lightweight drone-based pollution and weather sensors while offering low-noise measurements.

2.1 Overview

ASTRO+ is an environmental sensing platform that includes two main sensing technologies: ground reference sensors and aerial sensing using drones. We focus on measuring VOCs, which provide a good signature of both traffic and industry related air pollution. For reference ground sensing, we selected Defiant's FROG-5000, which uses gas chromatography to measure the four major VOC pollutants (Benzene, Toluene, Ethylbenzene, and Xylene) at the ppb level. Because reference measurement sensors such as the FROG-4000 are heavy and cannot be deployed easily on drones, we use **Photo Ionization Detection** (**PID**) VOC sensors for aerial measurements. PID sensors can weigh as little as 100 g and provide fast response measurements compared to other lightweight sensing solutions such as electrochemical sensors. After careful analysis of existing PID sensors, we selected ION Science's miniPID2 VOC sensor, which has limited temperature and humidity effects compared to other sensors in the market.

2.2 Architecture of ASTRO+

ASTRO+ includes three layers: sensing, data storage, and a third layer for data visualization and user notification as shown in Figure 1. Data that is collected by both drones (PID sensors) and ground sensors (gas chromatography in addition to PID) is sent over WiFi to an Internet-hosted database. The database is connected to a mobile app and a web service that allow community users to visualize both real-time measurements and historical data. In addition to raw measurements of both ground sensors and last drone missions, the mobile app also indicates the air quality based on EPA's air pollution thresholds. In addition to data visualization, users can subscribe to SMS and E-mail notifications in order to be informed in real time about pollution peak levels.

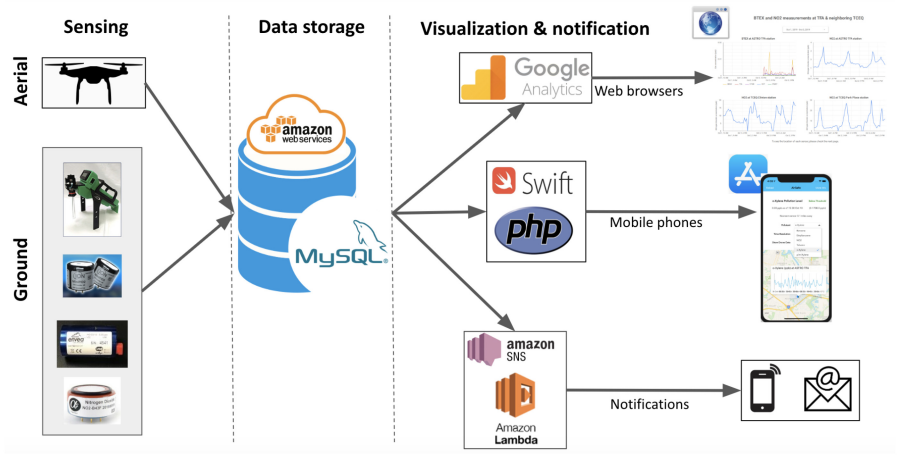

Fig. 1. Architecture of *ASTRO+*.

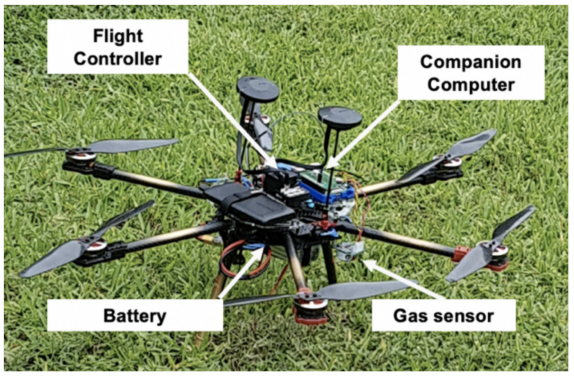

Fig. 2. *ASTRO+* UAV system.

2.3 UAV System

We build our UAV-based sensing system as an extension of our *ASTRO* platform [17, 21]. *ASTRO* is a UAV network platform that is *Autonomous* and *Tetherless* in the sense that drones form an infrastructureless wireless network and don't need a base station to make their sensing decisions. Due to using carbon fiber lightweight frames, *ASTRO* drones allow up to 15 min flight time and up to 1.5 kg of payload. *ASTRO* also uses hardware components that are widely used within the open source community, namely, the *Pixhawk* flight controller to manage the avionics part and the *Raspberry Pi* as a companion computer in order to manage the network communication part.

We extend *ASTRO* by deploying lightweight VOC, temperature, humidity, and wind sensors while offering low-noise measurements. This is achieved by first locating the sensors right next to center of the drone as shown in Figure 2 in order to minimize turbulence effects that are caused by the propellers [24]. In addition to that, we isolate the power source of the environmental sensors from the flight controller and companion computer battery in order to maintain the stability of the input voltage of the sensors. Gas, temperature, humidity, and wind measurements are

Fig. 3. Experimental setup.

performed once per second due to the fast response of the selected sensors. In terms of resolution, temperature values are reported within ±1° Celsius, relative humidity is reported within ±1%, and VOC measurements are reported at the ppb level.

3 EVALUATION OF AERIAL SENSING ERRORS

In this section, we use the aerial and reference ground sensors of *ASTRO+* to analyze the quality of aerial measurements of VOCs. Prior work suggested that the dynamic airflow created by drones' propellers affects the quality of the measurements. However, it is not previously known how these dynamics affect the sensing mechanism of drone-mounted pollution sensors. Indeed, the main lightweight gas sensing technologies (photoionization-based and electrochemical sensors) can be easily affected by changes in weather conditions such as temperature and humidity but not necessarily the airflow and wind velocity [15]. In this section, we propose a fine characterization of these effects using an experimentally collected dataset.

3.1 Experimental Scenario

We performed multiple data collection experiments in Milby Park (Houston, Texas), a residential neighborhood that is highly exposed to both traffic pollution (facing a highway) and industrial pollution (located within less than 2 miles of three chemical plants). We collected in different locations and times during *February* and *October* 2020 more than 2,000 measurements of both ground reference data and aerial data of VOC pollution concentrations in addition to aerial data of temperature, relative humidity, and wind velocity.

As depicted in Figure 3, each measurement was performed while having the drone hovering at about 2.5 m and located within 4 to 5 meters of the ground sensor, which was sampling at an altitude close to that of the drone (1.5 m). In order to reduce sensing errors during the measurement campaign, and as recommended by manufacturers [20, 29], both aerial and ground sensors were properly calibrated in the field against reference gas concentrations of Isobutylene (a VOC gas that is commonly used to calibrate PID sensors).

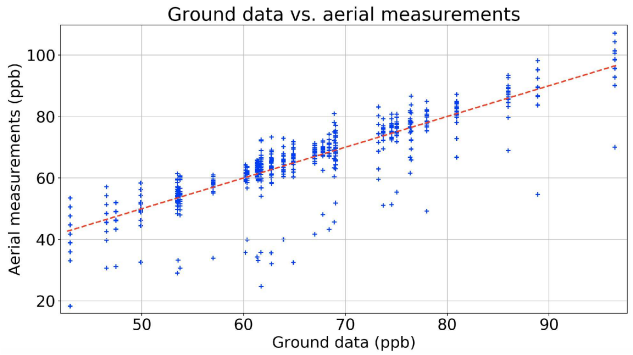

Fig. 4. Ground measurements vs. aerial measurements.

3.2 First Analysis

Figure 4 depicts the obtained VOC ground measurements on the x-axis and the corresponding aerial measurements on the y-axis. Note that even though aerial measurements may underestimate the real concentrations in some few cases going down to as low as 20 ppb compared to the lowest reference concentration of 40 ppb, the overall bias of drone data is very low and does not exceed 1 ppb due to the proper calibration of the sensors prior to the measurement campaign. However, the overall standard deviation of aerial sensing errors is substantial and exceeds 6% of the full range of the measured concentrations (96 ppb). This is clearly due to the dynamic nature of aerial measurements where drone propellers' effects are very variable and therefore difficult to predict.

In order to characterize the main sources of aerial measurement errors, we depict in Figure 5 the standard deviation of the error of aerial measurements with respect to ground reference data depending, respectively, on wind velocity (generated by the drone propellers), temperature, relative humidity, and absolute humidity. We recall that all temperature, humidity, and wind sensors all located on top of the drone and measure the ambient air that is surrounding the drone pollution sensor. The air flow speed generated by the propellers seems to have a low but still existing correlation, which does not exceed 25%. However, temperature and relative humidity dynamics (which are caused in part by the airflow dynamics that are due to the propellers' wind) correlate with aerial measurements' quality better than wind and yield more than 60% of linear correlation and more than 90% of polynomial third-order correlation. This is mainly due to the high sensitivity of pollution sensors in general to temperature [15], and also the sensitivity of PID sensors in particular to the level of water vapor in the air [23]. This is why water vapor (also defined as absolute humidity and calculated based on both temperature and relative humidity) provides almost 90% correlation with aerial measurements quality when using just the first-order polynomial fit.

3.3 Evaluation of Inference Models

As already highlighted, on-drone air pollution measurement errors exhibit remarkable correlations with temperature and humidity. In this section, our objective is to evaluate different inference models where the output is the quality of pollution aerial measurements (i.e., error's standard deviations) based on the data of temperature, humidity, and wind sensors. While using cross validation and considering the mean squared error as our inference loss function, we divide our 2,000 collected measurements' dataset into five groups. We report in Table 1 the inference accuracy level (R^2) of (i) single linear regression, (ii) **multiple linear regression** (MLR) in addition to

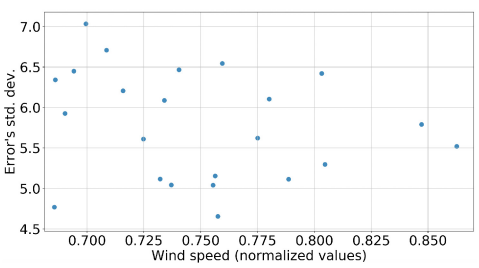

(a) Effects of wind velocity

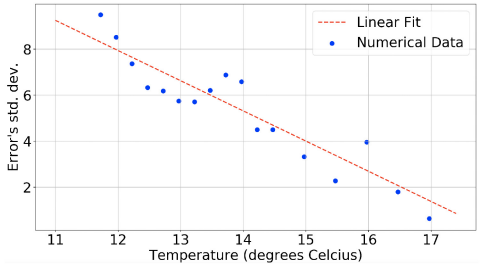

(b) Effects of temperature

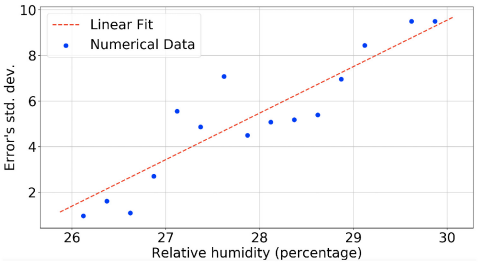

(c) Effects of rel. humidity

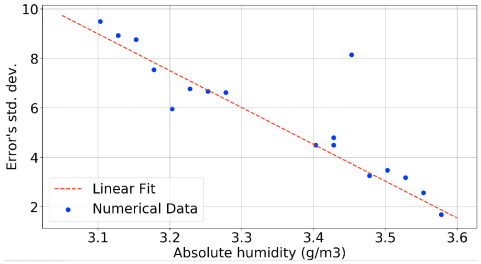

(d) Effects of abs. humidity

Fig. 5. Effects of wind, temperature, and humidity on the quality of VOC aerial measurements.

Table 1. Evaluation Results of Inference Models

R^2 (%)	Single linear regression				MLR	SVM	DNN
	Wind	Temp.	R. hum.	Abs. hum.			
Avg.	23%	64%	65%	87%	66%	94%	94%
Max.	25%	67%	68%	89%	70%	95%	96%
Min.	21%	58%	63%	85%	63%	93%	92%

(iii) **support vector machines** (**SVMs**), and (iv) **deep neural networks** (**DNNs**), which have been proven in the literature as very efficient nonlinear regression solutions [1]. Note that absolute humidity is not considered as an input to the MLR, SVM, and DNN inference models due to the fact that it is a redundant inference input. Indeed, absolute humidity is not a measured value but rather calculated based on temperature and relative humidity measurements.

The results presented in Table 1 confirm the efficiency of linear regression when using absolute humidity values, which yields up to 89% accuracy in the five groups of the cross-validation process. Note that this is even better than performing a multiple linear regression that uses temperature, relative humidity, and wind raw measurements, in which case the performance accuracy does not exceed 70%. This is because absolute humidity is—by definition—a non-linear combination of temperature and relative humidity and hence reflects in a better way the non-linear effects of temperature and relative humidity on pollution measurements. However, SVM regression and DNN, which allow on average around 94% inference accuracy, better handle these non-linearities by learning the best non-linear combination of temperature and relative humidity as opposed to the fixed formula of absolute humidity.

Discussion. The results presented in this section show that co-locating temperature, humidity, and wind sensors with air pollution sensors can help infer the quality of pollution aerial

measurements subject to a proper training prior to environmental mapping missions. For instance, and as shown in this section, PID measurements' quality can be inferred to almost 90% using absolute humidity data (calculated based on temperature and relative humidity measurements). For other pollution sensors (electrochemical sensors, for instance), the predictive variables can be different than absolute humidity or a combination of multiple weather conditions but the correlation should still remain high as most air pollution sensors are very sensitive to weather conditions [15]. This measurements' quality inference fact can then be used to characterize pollution aerial sensing quality at future measurement locations by first interpolating the already collected weather data and then using the results of this interpolation to predict pollution measurements' quality at future sensing points.

Based on the results of this section, we propose to classify the evaluated inference models into three groups:

(i) Accurate inference models (SVM, DNN, and single linear regression based on absolute humidity), which allow an inference accuracy that is greater than 85%.
(ii) Average inference models (linear regression based on either temperature, humidity, or both), which allow an inference accuracy that is between 50% and 70%.
(iii) Poor inference models (single linear regression based on wind velocity measurements), where the inference accuracy is less than 30%.

We compare later in Section 5 the impact of using these different inference models on the overall performance of UAV mission planning.

4 ROBUST MISSION PLANNING FOR AIR POLLUTION MAPPING

4.1 Overview

The experimental study presented in the previous section confirms that pollution aerial measurements' quality is dynamic and non-homogeneous with respect to the measurement context (temperature, humidity, and wind levels of the ambient air). These dynamics should have a direct impact on the performance of UAV mission planning algorithms since low-quality measurements may lead to a poor estimation of the drones' mission plans. Based on that fact, we design in this section a UAV mission planning approach while relying on a fine characterization of aerial measurementsâ.. quality in addition to the inherent pollution spatial correlations. Given an input region to be monitored and a set of pollution-sensing UAVs with limited flight time, we aim at (i) determining a selection of points that should be sampled by the UAV network so that the obtained measurements yield a low-error estimated pollution map; and (ii) determining for each UAV the locations that should be visited so that the covered points of interest are visited by at least one drone. Here, the estimated pollution map is obtained by interpolating the data collected at the optimal measurement locations.

The proposed mission planning approach operates as follows: after a training phase prior to the flight mission in order to quantify the impact of temperature, humidity, and wind velocity on aerial measurements of pollution concentrations, UAVs are first sent to uniformly distributed locations in order to characterize the spatial correlations of air pollution concentrations. Then, these spatial correlations are used together with the inferred aerial measurements' quality in order to optimize the following measurement locations of the drones. The optimal measurement locations of each drone are obtained by minimizing the overall variance of the interpolated concentrations' errors while taking into account the aerial sensing constraints (the dynamic sensing error and the response time of pollution sensors, the speed of the drone, and the drone's battery capacity).

Table 2. Main Notations Used in our Approach

	Description	Dimension
$\boldsymbol{p}$	Space points	$l \times 1$
$\boldsymbol{g}$	*Unknown* ground truth vector	$l \times 1$
$\boldsymbol{z}$	Measurements' vector	$n \times 1$
$\boldsymbol{c}$	Interpolated concentrations' vector	$l \times 1$
H	Measurements-to-Space mapping matrix	$n \times l$
$\boldsymbol{\theta}$	Vector of random sensing errors	$n \times 1$
B	Correlation matrix of pollution concentrations	$l \times l$
R	Covariance matrix of sensing errors	$n \times n$
F	Covariance matrix of interpolation errors	$l \times l$
W	Interpolation weights' matrix	$l \times n$

4.2 Air Pollution Mapping

Before getting into the details of our UAV mission planning process, we first present the mathematical formulation that allows us to estimate pollution concentrations at unmeasured locations given a set of space locations with a limited number of measurements. We focus on the optimal linear interpolation method, which is the most used air pollution data interpolation technique in the literature [25]. Without loss of generality, and due to the relatively short flight time of drones, we focus on the case of pollution concentrations that change only in space and not in time. The main notations used in this section are summarized in Table 2.

Let $\boldsymbol{p}$ be a vector of l discrete points approximating the space in 2D or 3D, i.e., $\boldsymbol{p} = [p_1, p_2, \ldots, p_l]^T$ where $p_i = (x_i, y_i, z_i)$. We use $\mathbf{g} \in \mathbb{R}^l$ to denote the unknown ground truth timely static pollution concentrations at the l points of space. i.e., $\mathbf{g} = [g_1, g_2, \ldots, g_l]^T$ where g_i is the pollution concentration at point i. Let $\boldsymbol{z} \in \mathbb{R}^n$ be a set of measurements performed at n different locations in space $\boldsymbol{p}$, i.e., $\boldsymbol{z} = [z_1, z_2, \ldots, z_n]^T$ where z_i is measurement number i. In order to map measurements to space locations, we define a matrix $H \in \mathbb{R}^{n \times l}$ where each matrix element h_{ij} is a Boolean set to 1 if measurement number i is performed at point j. Let θ_i be the error of measurement z_i with respect to ground truth g_i. We denote the variance of sensing error θ_i using r_i, which can be inferred based on co-located measurements of temperature, humidity, and wind velocity as demonstrated in the previous section of this article. In addition, we assume that θ_i has a zero mean as this is usually the case when pollution sensors are properly calibrated. We also assume that pollution measurement errors are uncorrelated because they mainly depend on the electronics of the sensing mechanism. Hence, the covariance matrix of sensing errors, $R \in \mathbb{R}^{n \times n}$, is a diagonal matrix.

Air pollution concentrations g_i are inherently correlated in space [25]. We denote the spatial correlation matrix of pollution concentrations by $B \in \mathbb{R}^{l \times l}$. Each matrix element b_{ij} reflects for space locations i and j the probability of being at the same concentration level.

Using the measurement vector $\boldsymbol{z}$ and the matrix H defining measurement locations, our objective is to obtain an estimation vector $\boldsymbol{c} \in \mathbb{R}^l$ by interpolating pollution concentrations at unmeasured locations. In the case of optimal linear interpolation [11], $\boldsymbol{c}$ is defined in matrix form as

$$\boldsymbol{c} = W\boldsymbol{z}$$

such that $\boldsymbol{c}$ is a linear combination of the collected measurements. The interpolation weights are defined by the matrix W, which is calculated as in [11],

$$W = BH^T(R + HBH^T)^{-1}, \tag{1}$$

and is a function of sensing quality defined by matrix R in addition to the spatial correlation matrix of pollution concentrations B. Let η_i denote the interpolated concentrations' errors with respect to the unknown ground truth value at each point i (i.e., $\boldsymbol{\eta} = \boldsymbol{c} - \boldsymbol{g}$). The covariance matrix of $\boldsymbol{\eta}$ (denoted F) is calculated as in [11],

$$F = (I_l - BH^T(R + HBH^T)^{-1}H)B, \tag{2}$$

where I_l is the identity matrix. Based on F, we define the overall mapping error of a given interpolated map $\boldsymbol{c}$ corresponding to a given measurements' vector $\boldsymbol{z}$ as

$$\sum_{i \in [1,l]} c_i^{\alpha} \times f_{ii},$$

where α is a parameter used to emphasize the interpolation error at polluted locations compared to the slightly polluted ones. Indeed, the higher the value of the α parameter, the higher is the contribution of the polluted locations (locations i where c_i is high) in the sum of the optimization function.

4.3 Mission Planning Process

We consider a mobile sensing system consisting of m drones that are equipped with air pollution sensors that are used to collect measurements $\boldsymbol{z}$ within the monitoring region $\boldsymbol{p}$. In order to quantify the covariance matrix of pollution measurements' errors R, drones are also equipped with temperature, humidity, and wind sensors. This allows us to infer on-the-fly r_i, the error variance of each already collected measurement z_i in addition to inferring the measurement error variance at future mission locations by interpolating the already collected temperature, humidity, and wind data. The measurement error inference is obtained based on a training phase that is performed prior to the pollution mapping mission by co-locating drones and reference sensors as shown in Section 3.

Because of the response time of pollution sensors, drones need to hover for a time $\mathcal{T}_{hover}$ in order to obtain a pollution measurement at a given space point [15]. In addition to the hover time constraint, we assume that drones travel at a constant speed v. Based on that, we calculate the travel times between each pair of points (i, j) that we denote by $\mathcal{T}_{travel}(i, j)$. In addition, let $\mathcal{T}_{flight}$ be the maximum flight time of each drone, which mainly depends on the weight of the drone, the capacity of the battery, and the drone speed v.

In terms of communication, we assume that drones remain connected to the base station when traveling within the monitoring region $\boldsymbol{p}$. This is usually the case in urban environments and industrial areas. In addition, we assume that the communication delay between the drones and the base station is minimal compared to the measurement hover time of the drones, which can be as high as 30 s [15].

Our mission planning approach operates in two phases: a learning phase and an optimization phase. The objective of the first phase is to learn the spatial correlation matrix of pollution concentrations B. In the second phase, we define and solve an optimization model while relying on spatial correlations B and non-homogeneous measurements' quality R in order to guide the drones to the locations that allow us to obtain a vector $\boldsymbol{c}$ of estimated concentrations with a corresponding covariance matrix F where the mapping quality defined in the previous section ($\sum_{i \in [1,l]} c_i^{\alpha} \times f_{ii}$) is minimized.

Phase 1: Initialization phase. Our objective in phase 1 is to characterize the spatial correlations of pollution concentrations by estimating the matrix B. To that end, we perform n_0 measurements that are uniformly distributed in the monitoring region. We first divide the monitoring region into m sub-regions having the same surface area. Each drone is then sent to one of these

sub-regions and performs n_0/m uniformly distributed measurements. Note that n_0 is a parameter that should be chosen carefully depending on the size of the monitoring region. At the end of phase 1, the obtained pollution measurements, denoted by $\boldsymbol{z^0}$, in addition to the inferred measurements' quality matrix R, are sent over to the base station. Based on that data, the base station performs the characterization of the spatial correlations as explained later in Section 4.4 and mission planning decisions as explained in Section 4.5.

Phase 2: Optimization phase. Our objective in phase 2 is to use the obtained B matrix in order to find the best way-points where drones should perform their measurements while taking into account flight time constraints. The optimization algorithm is run at the base station at the end of the initialization phase. As a result, each drone obtains the optimal mission plan with respect to the current characterization of pollution spatial correlations. Each drone follows then the provided mission plan and each performed measurement is sent right away to the base station. The latter uses the new data in order to refine the characterization of pollution spatial correlations at a specific rate. The new characterization of spatial correlations is then used to refine the optimal mission plans of the drones and this process continues until no more data can be performed. At the end, the base station uses the full set of the obtained measurements combined with the inferred sensing quality and the final characterization of pollution spatial correlations in order to calculate the final interpolated concentrations $\boldsymbol{c}$.

4.4 Robust Spatial Correlation Characterization

Given a set of already collected measurements $\boldsymbol{z^0} \in \mathbb{R}^{n_0}$ in addition to online inferred measurements' quality R, our aim is to estimate the pollution spatial correlations B. We recall that each matrix element b_{ij} corresponds to the correlation between the *unknown* ground truth concentrations g_i and g_j. In order to estimate the pollution spatial correlation between each pair of locations i and j, we first define as $D(i,j)$ the set of sampled location pairs that are within a Euclidean distance close to the distance between locations i and j. Mathematically, the set $D(i,j)$ can be written as

$$D(i,j) = \{(a,b) \mid z_a, z_b \in \boldsymbol{z^0} \ \ \& \ \ \|p_a - p_b\| = \|p_i - p_j\| \pm \Delta\}.$$

Based on $D(i,j)$, we estimate the b_{ij} spatial correlation as

$$b_{ij} = corr\left(\begin{bmatrix} \frac{z_{a_1}}{r_{a_1}+r_{b_1}} \\ \vdots \\ \frac{z_{a_{|D|}}}{r_{a_{|D|}}+r_{b_{|D|}}} \end{bmatrix}, \begin{bmatrix} \frac{z_{b_1}}{r_{a_1}+r_{b_1}} \\ \vdots \\ \frac{z_{b_{|D|}}}{r_{a_{|D|}}+r_{b_{|D|}}} \end{bmatrix}\right). \tag{3}$$

This provides a robust estimation of $corr(g_i, g_j)$ while taking into account measurement errors by normalizing the measurements within each pair of points (a,b) using their respective error's variance r_a and r_b. The outcome of this normalization process is that low-quality measurements (i.e., pairs (a,b) where either r_a or r_b is high) become less involved in the final estimated correlations b_{ij}, whereas high-quality measurements (i.e., pairs (a,b) where both r_a and r_b are low) are emphasized.

4.5 Robust Mission Planning Optimization

Using the obtained characterization of spatial correlations B and the inferred measurements quality matrix R, our objective is to find the best locations that offer the best interpolation of pollution concentrations. In addition, we ensure that the selected locations can be sampled with the m drones subject to their remaining flight time $\mathcal{T}_{flight}$. We determine for each drone the best ordered set of

sampling points by solving the following optimization model:

$$\textbf{Minimize} \quad \sum_{i \in [1,l]} c_i^{\alpha} \times f_{ii}$$
$$\textbf{Subject to} \quad \text{Eq. (1), Eq. (2), and flight constraints}$$

The objective function ensures the minimization of the overall variance of estimated concentration errors f_{ii}, $i \in [1, l]$ while emphasizing the interpolation error at polluted locations compared to the slightly polluted ones. The minimization of the interpolation error's variance is performed with respect to the matrix H, which is the main decision variable in the optimization process and defines the best aerial sensing locations. In order to take into account the aerial sensing requirements, we constrain the sensing locations so that they are ordered in a way that takes into account the necessary sampling hover time in addition to drone travel times when moving from one location to another.

We solve our mission planning optimization model using commercial optimization solvers (IBM CPLEX) in the case of small monitoring regions. In order to scale our approach to large regions, we propose to solve the optimization model to obtain only a partial mission plan for each drone and then update the mission plans as the drones are flying.

5 EXPERIMENTAL EVALUATION OF ROBUST MISSION PLANNING

In this section, we first use a real-world dataset in order to validate the efficiency of our robust mission planning, which leverages the use of co-located weather sensors to infer the aerial sensing quality of pollution concentrations and guide the drones to the most accurate measurement locations. We show that we reach a high performance even with average sensing inference models. Then, in the second part of this section, we use a numerically generated dataset in order to explore the impact of the dynamics of both pollution concentrations and aerial sensing quality on the overall performance of our mission planning approach. We conclude that the efficiency of our optimization approach remains high even in the presence of heterogeneous pollution fields and sensing qualities.

5.1 Experimental Setup

Dataset. We evaluate our mission planning approach using a set of 30 pollution maps of aerial and ground measurements of VOC pollutants collected in February and October 2020 using our sensing platform *ASTRO+*. We also use as input the collected weather data (temperature, humidity, and wind) in order to infer online VOC sensing errors. By default, we consider the application of the linear sensing inference model that is based on absolute humidity since the latter is highly correlated with aerial pollution measurement qualities as shown in Section 3. Each collected data map corresponds to a grid of 34 data points ($l = 34$) within the Milby Park residential neighborhood (Houston, Texas). Figure 6 illustrates an example of the spatial distribution of the main input maps (respectively, an aerial VOC map collected by the drone, a VOC ground map collected by a reference sensor, and aerial absolute humidity data).

Flight constraints. We assume that drones fly high enough to avoid obstacles and that their flight speed is fixed at 2 m/s for safety reasons. We set the hover time of each drone to 10 s since we are focusing on VOC sensors, which have an acceptable response time that is usually within few seconds. We consider flight times of up to 40 min where the first 10 min are reserved to the initialization phase of our mission planning approach. This allows us to perform six uniformly distributed initial measurements ($n_0 = 6$), which is necessary for an initial characterization of pollution spatial correlations matrix B.

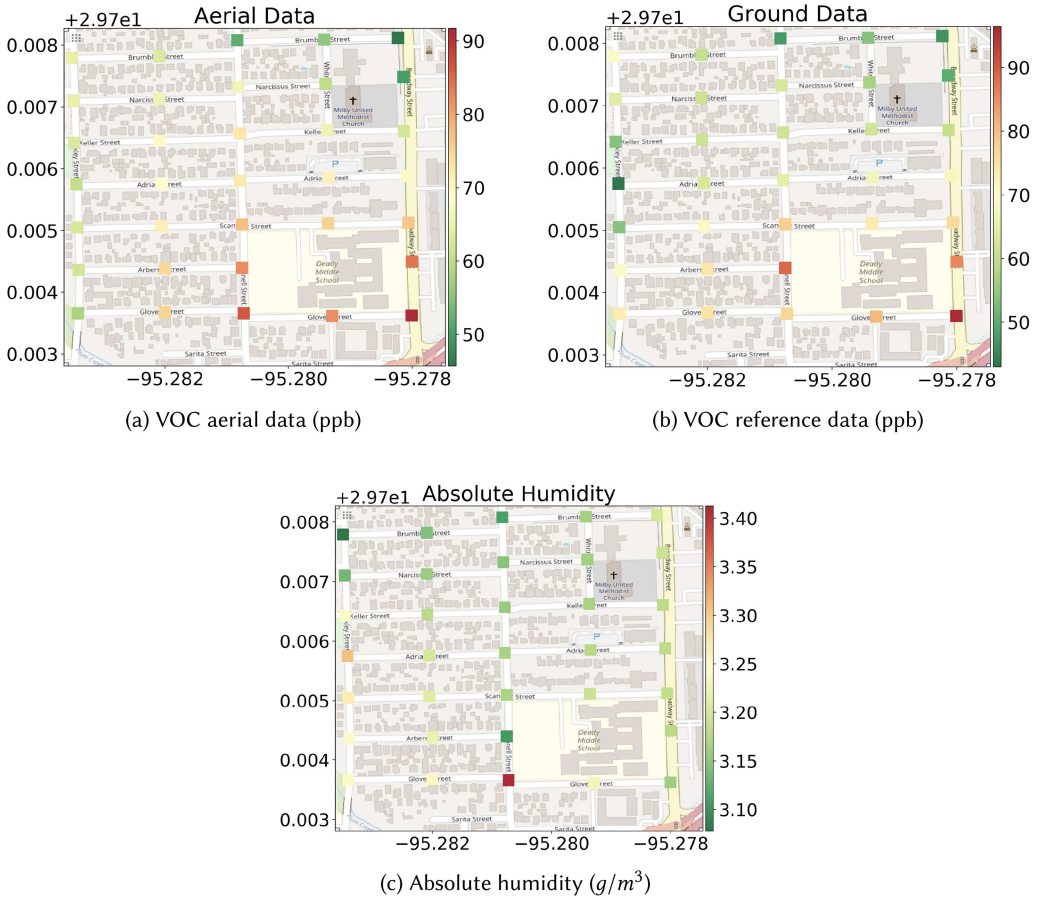

(a) VOC aerial data (ppb)

(b) VOC reference data (ppb)

(c) Absolute humidity (g/m^3)

Fig. 6. Mission planning evaluation dataset (one map example).

Performance metric. We simulate our mission planning approach while using the aerial data maps each time a drone sample is performed. Then we evaluate the quality of the output of each simulation by comparing the final interpolated map of aerial data to the corresponding reference ground map. We use the relative RMSE as a performance metric to evaluate the percentage of interpolation error of each environmental sensing mission.

Performance benchmarks. We compare the results of our robust mission planning to the following baselines:

— *Omniscient planning:* this is the optimal trajectory that can be followed to get the best interpolation results, and can be obtained while relying on the exact error of aerial measurements (assumed to be hypothetically known). Given a number of sampling locations to optimize, we perform an exhaustive search to find the best combination of measurement locations that minimize the RMSE evaluation metric.

— *Traditional mission planning:* in this case, the measurement error's variance is assumed homogeneous and provided by the manufacturer as in most prior work. To evaluate this case, we simulate our optimization approach while setting the measurement error's variance r_i of each point i to the overall sensing errors' variance (36 ppb^2 in our VOC dataset).

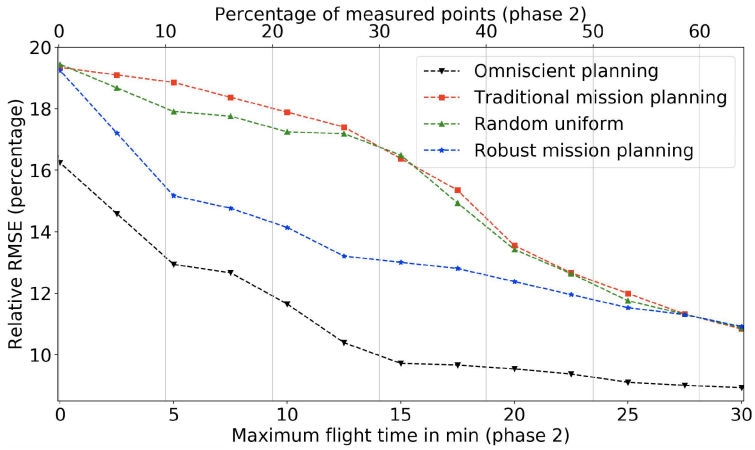

Fig. 7. Robust mission planning performance compared to baselines.

— *Random uniform:* this corresponds to flying the drone to random sensing locations following the uniform distribution.

5.2 Validation Results

Figure 7 depicts the results obtained while considering a single drone with an overall flight time of up to 40 min, which allows the drone to sample on average up to 25 locations including the measurements collected during the 10 min of the initialization phase.

The results show that due to the dynamic and non-homogeneous nature of aerial sensing quality, traditional mission planning fails to send the drones to the most informative locations and selects instead measurement locations that are almost uniformly distributed in the monitoring region. This is due to the optimization objective function of traditional mission planning which only depends on spatial correlations since the variance of sensing errors is assumed homogeneous. Compared to that, and due to taking into account the heterogeneous nature of aerial sensing errors, our approach adjusts the spatial density of selected measurement locations depending on the sensing quality. This helps first better characterize the spatial correlations of pollution concentrations and then improve the interpolation performance by using the most accurate aerial data. As a result, our robust mission planning outperforms traditional solutions by up to 2.5× improvement factor (calculated with respect to the omniscient planning).

Note that our performance improvement decreases as the drone's flight time is extended. This is due to the small size of the monitoring region (500 m × 500 m), where a 30 min flight time in the second phase (40 min including phase 1) allows a single drone to sample more than half of the grid points and as a result obtain a good interpolation quality even with uniformly distributed measurement locations. However, our approach, being efficient even with limited sensing resources (2.5× improvement factor with just 10% of sensing resources), allows us to efficiently monitor large deployment regions.

The efficiency of our robust planning both in terms of achievable performance improvement factor and required sensing resources may depend on three main parameters: (i) the accuracy of sensing inference models, which—if not good enough—may invalidate the accuracy of our mission plans; (ii) the dynamics of pollution concentrations; and (iii) the spatial dynamics of sensing errors, which may lead to low correlations between measurement locations and therefore reduce the

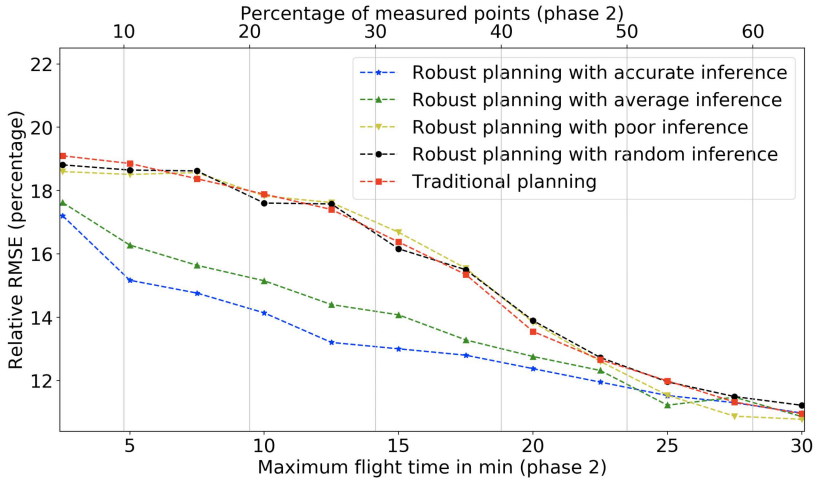

Fig. 8. Impact of the accuracy of sensing inference models.

performance of the interpolation process. We explore these three performance parameters in the following of this section.

5.3 Impact of the Accuracy of Sensing Inference Models

We focus in this section on how the performance of our robust mission planning scales with the accuracy of the inference model that is used to predict the quality of aerial measurements of pollution concentrations. We recall that in Section 3, we identified three inference model groups where the inference accuracy is either greater than 85% (accurate), between 50% and 70% (average), or less than 30% (poor). Figure 8 depicts the average performance results of our mission planning depending on sensing resources while considering accurate, average, and poor inference models compared to traditional planning. For comparison purposes, we also plot in Figure 8 the results obtained with our planning approach when considering random uniform sensing inference.

We first observe that even with an average inference model, our mission planning outperforms traditional solutions and allows up to 2× improvement factor. Most importantly, dropping the sensing inference quality from 95% (using SVMs) to 65% (using temperature-based linear regression) involves a performance drop that is less than the accuracy ratio of those two inference models. In addition, the performance improvement when using average sensing inference follows the same convex pattern of robust planning that is based on accurate sensing inference. Indeed, in the mission planning optimization process, the most important thing is to identify inaccurate measurement locations and not necessarily estimate the exact quality of the aerial measurements.

The comparison between the impact of accurate and average inference models also shows that the importance of the sensing inference model is higher in the early stage of the mission planning process: as the drones fly and more data is collected, the quality of the inference model becomes less important as there are less locations to select (smaller search space).

Figure 8 also shows that using a poor inference model (such as a wind-based linear regression or even random inference) yields similar performance compared to traditional planning but not worse. The reason behind that is that although poor inference models assign wrong sensing quality to aerial measurements, the range of the sensing errors is preserved, and as a result, poor inference models are close to estimating that sensing errors are homogeneous as in the case of traditional planning.

Table 3. Default Simulation Parameters

Parameter	Notation	Value
Number of space points	l	100
Mean of pollution concentrations	$\mu_{\boldsymbol{g}}^2$	50 ppb
Variance of pollution concentrations	$\sigma_{\boldsymbol{g}}^2$	15^2
Mean of humidity levels	$\mu_{\boldsymbol{a}}^2$	50%
Variance of humidity levels	$\sigma_{\boldsymbol{a}}^2$	5^2

5.4 Impact of the Dynamics of Pollution Concentrations and Sensing Quality

As already highlighted, the robustness of our mission planning approach is dependent upon the dynamics of pollution concentrations and the spatial dynamics of sensing errors, which have a direct impact on the performance of the interpolation process. Since these dynamics cannot be controlled in our experimental dataset, we explore their effects using numerically generated environmental data inputs (pollution concentrations and weather data) while considering different heterogeneity levels. We first present our numerical scenario using the same notations as in Section 4 and then discuss the obtained numerical results.

5.4.1 Numerical Scenario. We consider a 2D space with an area of (500 m × 500 m) associated with a uniform grid $\boldsymbol{p}$ of 100 space points ($l = 100$). We simulate pollution ground truth concentrations and weather data as Gaussian processes, which is a very common simulation approach for environmental data [13]. For simplification purposes, we assume that the mean and the variance of the pollution field $\boldsymbol{g}$ are stationary. That is,

$$\boldsymbol{g} \sim \mathcal{N}\left(\mu_{\boldsymbol{g}} 1_l, \sigma_{\boldsymbol{g}}^2 B\right),$$

where $\mu_{\boldsymbol{g}}$ and $\sigma_{\boldsymbol{g}}^2$ are, respectively, the stationary mean and variance of the ground truth pollution field, $1_l \in \mathbb{R}^l$ is a vector with all elements set to 1, and B is the spatial correlation matrix of pollution concentrations.

In order to isolate the main input parameters that we are investigating in this section, we derive the B matrix using a distance-decay exponential function and assume that it is perfectly known during the mission planning process without a required initialization phase.

In addition to the pollution ground field $\boldsymbol{g}$, we simulate weather data (mainly humidity levels $\boldsymbol{a} \in \mathbb{R}^l$) as

$$\boldsymbol{a}_i \sim \mathcal{N}\left(\mu_{\boldsymbol{a}}, \sigma_{\boldsymbol{a}}^2\right) \ \forall i \in [1, l] \ i.i.d.,$$

where $\mu_{\boldsymbol{a}}$ and $\sigma_{\boldsymbol{a}}^2$ are, respectively, the mean and the variance of the humidity distribution.

We recall that the aerial sensing error at a point i is denoted using θ_i. We assume that θ_i variables are independent and defined as

$$\theta_i \sim \mathcal{N}(0, r_i),$$

where r_i is the variance of θ_i and is assumed to be a perfect linear function of the humidity level at point i; i.e., $r_i = u(a_i)$. Therefore, we simulate the aerial sensing errors θ_i based on humidity levels a_i as

$$\theta_i \sim \sum_{1}^{u(a_i)} \mathcal{N}(0, 1).$$

We explore in the following of this section the impact of the dynamics of pollution concentrations and sensing errors by varying mainly $\sigma_{\boldsymbol{g}}^2$ and $\sigma_{\boldsymbol{a}}^2$. The default parameters of the simulation process are summarized in Table 3.

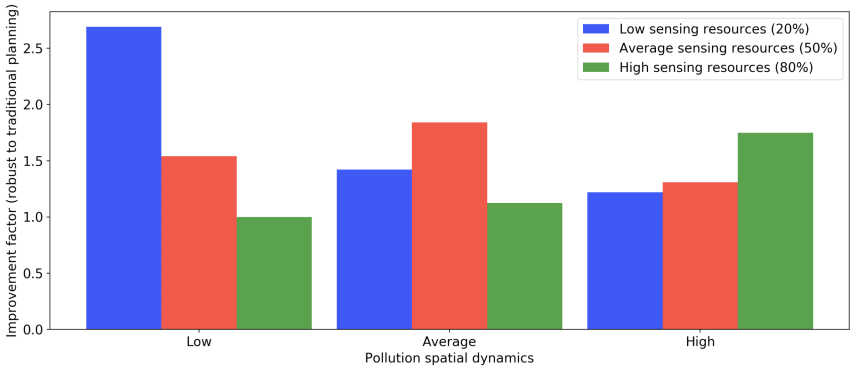

Fig. 9. Impact of the spatial dynamics of pollution concentrations.

5.4.2 Evaluation of the Impact of the Dynamics of Pollution Concentrations. In order to explore the effects of the heterogeneity level of ground pollution concentrations on the performance of robust planning, we vary the variance of the Gaussian field $\boldsymbol{g}$ while considering three configurations: (i) low spatial dynamics with $\sigma_{\boldsymbol{g}} = 5$, (ii) average spatial dynamics with $\sigma_{\boldsymbol{g}} = 15$, and (iii) high spatial dynamics with $\sigma_{\boldsymbol{g}} = 25$.

We run both our robust mission planning and the traditional optimization approach (100 simulation runs) and report in Figure 9 the average improvement factor at three different stages of the environmental missions (at the early stage where only 20% of the measurement locations have been sampled, in the middle of the mission, and at the final stage where 80% of the measurement locations have been sampled).

We first observe in Figure 9 that the overall improvement factor is at its highest value and exceeds 2.5× when the pollution dynamics are low. This is because the most important mission planning criterion in this case is the quality of aerial measurements, which are well inferred in our optimization approach.

We also observe that increasing the pollution dynamics does not involve decreasing the performance improvement with the same scale: the performance improvement remains at almost 2× even when pollution dynamics are high. The reason behind that is that selecting the best measurement locations has the same importance level as spatially distributing the measurements starting from a given threshold. It is noteworthy that however, the stage at which the highest performance is achieved changes depending on pollution dynamics and is reached only at the final stage in case of high pollution heterogeneity. Indeed, in this case, a higher number of measurements is necessary in order to achieve an efficient interpolation.

5.4.3 Evaluation of the Impact of Aerial Sensing Quality. We now focus on how the mission planning process is affected by the distribution of the aerial sensing errors. We recall that in our simulation process, the aerial sensing qualities are mainly derived from the distribution of humidity levels: the higher the humidity level, the lower the aerial sensing quality of pollution concentrations. Based on that, we vary in this simulation scenario the variance of humidity levels $\sigma_{\boldsymbol{a}}^2$ and consider three sensing configurations: (i) low pollution aerial sensing errors when $\sigma_{\boldsymbol{a}} = 1$, (ii) average pollution aerial sensing errors when $\sigma_{\boldsymbol{a}} = 5$, and (iii) high pollution aerial sensing errors when $\sigma_{\boldsymbol{a}} = 10$.

Since the sensing errors are well inferred in the robust mission planning, the obtained performance level is similar in our proposed approach. However, the performance of traditional planning highly varies in between the three aerial sensing scenarios that are considered in this evaluation

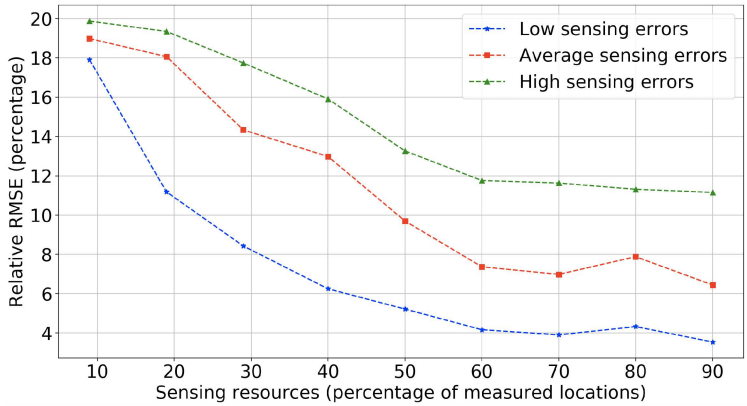

Fig. 10. Impact of aerial sensing quality on traditional planning.

test. In order to explore these variations, we report in Figure 10 the obtained relative RMSE of traditional planning while varying the available sensing resources (percentage of sampled locations).

The results in Figure 10 show that in all three sensing configurations, the relative RMSE of the interpolated pollution maps is reduced with increased sampled locations before converging to a plateau level, which happens when every other location is sampled and hence the sampled locations are already dense enough to provide an efficient interpolation. However, the curvature of the three different graphs in Figure 10 is highly dependent upon the dynamics of aerial sensing errors. Indeed, we observe that the performance curve of traditional planning tends to a concave form as the aerial sensing errors become higher and more dynamic. The reason behind that is that as the dynamics of aerial sensing errors increase, there is a higher probability of selecting sensing locations with inaccurate measurements if these errors are assumed to be homogeneous as in the case of traditional mission planning. As a result, in practice, the performance improvement of our mission planning process with respect to traditional planning is expected to increase with sensors aging as they become less accurate over time [23]. This means that our proposed mission planning approach also extends the overall lifetime of the aerial sensing system.

6 CONCLUSION

In this article, we propose a robust mission planning approach that adapts the trajectory of the drones while taking into account the quality of aerial measurements that is inferred from weather conditions. Compared to existing mission planning algorithms, we propose in our work to couple the pollution spatial correlations with a fine characterization of aerial measurementsâ.. quality in the optimization process of UAV mission planning. After a training phase prior to the flight mission in order to quantify the impact of temperature, humidity, and wind velocity on aerial measurements of pollution concentrations, our mission planning approach operates in two phases: a spatial-correlation-learning phase and a trajectory optimization phase. We evaluate our mission planning approach based on both experimental and numerically generated pollution datasets and show a high-performance improvement that is due to the fine characterization of the measurement errors. In terms of perspectives, we plan to extend the proposed mission planning approach to a distributed scenario in which the sensing locations of drones are optimized in a collaborative way.

ACKNOWLEDGMENTS

We thank the interns of the ASTRO team for their help with the experimental evaluation.

REFERENCES

[1] Kevin O. Achieng. 2019. Modelling of soil moisture retention curve using machine learning techniques: Artificial and deep neural networks vs support vector regression models. *Computers & Geosciences* 133 (2019), 104320.

[2] Amin Anjomshoaa, Fábio Duarte, Daniël Rennings, Thomas J. Matarazzo, Priyanka deSouza, and Carlo Ratti. 2018. City scanner: Building and scheduling a mobile sensing platform for smart city services. *IEEE Internet of Things Journal* 5, 6 (2018), 4567–4579.

[3] Amjed Belkhiri, Walid Bechkit, and Hervé Rivano. 2018. Virtual forces based UAV fleet mobility models for air pollution monitoring. In *2018 IEEE 43rd Conference on Local Computer Networks (LCN'18)*. IEEE, 481–484.

[4] Debarpan Bhattacharya, Sudip Misra, Nidhi Pathak, and Anandarup Mukherjee. 2020. IDeA: IoT-based autonomous aerial demarcation and path planning for precision agriculture with UAVs. *ACM Transactions on Internet of Things* 1, 3 (2020), 1–21.

[5] Ahmed Boubrima, Walid Bechkit, and Hervé Rivano. 2019. On the deployment of wireless sensor networks for air quality mapping: Optimization models and algorithms. *IEEE/ACM Transactions on Networking* 27, 4 (2019), 1629–1642.

[6] Ahmed Boubrima and Edward W. Knightly. 2020. Robust mission planning of UAV networks for environmental sensing. In *Proceedings of the 6th ACM Workshop on Micro Aerial Vehicle Networks, Systems, and Applications (ACM DroNet @ Mobisys)*. 1–6.

[7] Tauã Cabreira, Lisane Brisolara, and Paulo R. Ferreira. 2019. Survey on coverage path planning with unmanned aerial vehicles. *Drones* 3, 1 (2019), 4.

[8] Qijun Gu, Drew R. Michanowicz, and Chunrong Jia. 2018. Developing a modular unmanned aerial vehicle (UAV) platform for air pollution profiling. *Sensors* 18, 12 (2018), 4363.

[9] David Hasenfratz, Olga Saukh, Christoph Walser, Christoph Hueglin, Martin Fierz, and Lothar Thiele. 2014. Pushing the spatio-temporal resolution limit of urban air pollution maps. In *2014 IEEE International Conference on Pervasive Computing and Communications (PerCom'14)*. IEEE, 69–77.

[10] Gerard Hoek, Rob Beelen, Kees De Hoogh, Danielle Vienneau, John Gulliver, Paul Fischer, and David Briggs. 2008. A review of land-use regression models to assess spatial variation of outdoor air pollution. *Atmospheric Environment* 42, 33 (2008), 7561–7578.

[11] Eugenia Kalnay. 2003. *Atmospheric Modeling, Data Assimilation and Predictability*. Cambridge University Press.

[12] Reza Khodayi-mehr, Wilkins Aquino, and Michael M. Zavlanos. 2019. Model-based active source identification in complex environments. *IEEE Transactions on Robotics* 35, 3 (2019), 633–652.

[13] Andreas Krause, Carlos Guestrin, Anupam Gupta, and Jon Kleinberg. 2011. Robust sensor placements at informative and communication-efficient locations. *ACM Transactions on Sensor Networks (TOSN)* 7, 4 (2011), 31.

[14] Balz Maag, Zimu Zhou, and Lothar Thiele. 2018. A survey on sensor calibration in air pollution monitoring deployments. *IEEE Internet of Things Journal* 5, 6 (2018), 4857–4870.

[15] M. I. Mead, O. A. M. Popoola, G. B. Stewart, P. Landshoff, M. Calleja, M. Hayes, J. J. Baldovi, M. W. McLeod, T. F. Hodgson, J. Dicks, et al. 2013. The use of electrochemical sensors for monitoring urban air quality in low-cost, high-density networks. *Atmospheric Environment* 70 (2013), 186–203.

[16] Patrick P. Neumann. 2013. *Gas Source Localization and Gas Distribution Mapping with a Micro-drone*. Dissertation. Bundesanstalt fur Materialforschung und - prufung (BAM).

[17] Riccardo Petrolo, Yingyan Lin, and Edward Knightly. 2018. ASTRO: Autonomous, sensing, and tetherless netwoRked drOnes. In *Proceedings of the 4th ACM Workshop on Micro Aerial Vehicle Networks, Systems, and Applications*. 1–6.

[18] Juan Jesús Roldán, Guillaume Joossen, David Sanz, Jaime Del Cerro, and Antonio Barrientos. 2015. Mini-UAV based sensory system for measuring environmental variables in greenhouses. *Sensors* 15, 2 (2015), 3334–3350.

[19] Venkat Roy, Andrea Simonetto, and Geert Leus. 2016. Spatio-temporal sensor management for environmental field estimation. *Signal Processing* 128 (2016), 369–381.

[20] Francoise Sailhan, Valérie Issarny, and Otto Tavares-Nascimiento. 2017. Opportunistic multiparty calibration for robust participatory sensing. In *2017 IEEE 14th International Conference on Mobile Ad Hoc and Sensor Systems (MASS'17)*. IEEE, 435–443.

[21] Zhambyl Shaikhanov, Ahmed Boubrima, and Edward W. Knightly. 2020. Autonomous drone networks for sensing, localizing and approaching RF targets. In *2020 IEEE Vehicular Networking Conference (VNC'20)*. IEEE, 1–8.

[22] Hazim Shakhatreh, Ahmad H. Sawalmeh, Ala Al-Fuqaha, Zuochao Dou, Eyad Almaita, Issa Khalil, Noor Shamsiah Othman, Abdallah Khreishah, and Mohsen Guizani. 2019. Unmanned aerial vehicles (UAVs): A survey on civil applications and key research challenges. *IEEE Access* 7 (2019), 48572–48634.

[23] Rae Systems. 2013. *The PID Handbook: Theory and Applications of Direct-Reading Photoionization Detectors (PIDs)* (3rd Edition). Rae Systems.

[24] Tommaso Francesco Villa, Farhad Salimi, Kye Morton, Lidia Morawska, and Felipe Gonzalez. 2016. Development and validation of a UAV based system for air pollution measurements. *Sensors* 16, 12 (2016), 2202.

[25] David W. Wong, Lester Yuan, and Susan A. Perlin. 2004. Comparison of spatial interpolation methods for the estimation of air quality data. *Journal of Exposure Science and Environmental Epidemiology* 14, 5 (2004), 404–415.

[26] Yun Xiang, Lan S. Bai, Ricardo Pledrahita, Robert P. Dick, Qin Lv, Michael Hannigan, and Li Shang. 2012. Collaborative calibration and sensor placement for mobile sensor networks. In *2012 ACM/IEEE 11th International Conference on Information Processing in Sensor Networks (IPSN'12)*. IEEE, 73–83.

[27] Yuzhe Yang, Zijie Zheng, Kaigui Bian, Lingyang Song, and Zhu Han. 2017. Real-time profiling of fine-grained air quality index distribution using UAV sensing. *IEEE Internet of Things Journal* 5, 1 (2017), 186–198.

[28] Bo Zhang, Teng Xi, Xiangyang Gong, and Wendong Wang. 2019. Mutual information maximization-based collaborative data collection with calibration constraint. *IEEE Access* 7 (2019), 21188–21200.

[29] Qiuxi Zhu, Francoise Sailhan, Md Yusuf Sarwar Uddin, Valérie Issarny, and Nalini Venkatasubramanian. 2019. Multi-sensor calibration planning in IoT-enabled smart spaces. In *2019 IEEE 39th International Conference on Distributed Computing Systems (ICDCS'19)*. IEEE, 722–731.

Received July 2020; revised March 2021; accepted May 2021